

# Gravity.jl: Fast and accurate gravitational lens modeling in Julia

## I. Point-like and linearized extended sources

Marco Lombardi

University of Milan, Department of Physics, via Celoria 16, I-20133 Milan, Italy

Received \*\*\*date\*\*\*; Accepted \*\*\*date\*\*\*

### ABSTRACT

We present `Gravity.jl`, a new proprietary software for the modeling of gravitational lens systems. `Gravity.jl` is written in the Julia programming language, and is designed to be fast, accurate, and flexible. It can be used to model gravitational lens systems composed of multiple lensing planes, and to perform Bayesian inference on the lens model parameters. In this paper we present the theoretical and statistical ideas behind the code, and we describe its main features. In this first paper of the series, we focus on the modeling of point-like and small extended sources, for which we can linearize the lens equation. We show a practical use of `Gravity.jl` on a galaxy-scale lens, and we compare the results with those obtained with other codes. We also show how `Gravity.jl` can be used to perform Bayesian inference on cosmological parameters.

**Key words.** Gravitational lensing: strong, Methods: numerical, Methods: statistical

### 1. Introduction

The study of strong gravitational lenses, that is, massive objects such as galaxies or clusters of galaxies capable of significantly distorting the light coming from distant sources, represents both a unique opportunity and a formidable challenge for astrophysics. Gravitational lensing analyses continue to produce some of the most relevant scientific results in astrophysics. It is, in fact, undoubtedly the most powerful tool we have for robustly studying the total mass distribution of the galaxy or cluster of galaxies that act as a lens, and therefore it allows us to place very strong constraints both on the mass and on the possible presence of substructures through gravitational imaging techniques. In this way, very relevant information can be obtained on the properties of dark matter halos (see, e.g., Treu 2010). At the same time, the properties of the images produced by a gravitational lens, especially if the lens and the source are at redshift  $z \gtrsim 0.3$ , are influenced by the values of the cosmological parameters, such as the mass density, the dark energy density, and equation of state of the dark energy (see, e.g., Caminha et al. 2022). Therefore, systems with multiple images of sources at multiple redshifts, such as galaxy clusters, are very well suited to be used for cosmological studies. Moreover, in the last decade, it has been shown that in the case of variable sources (such as quasars or supernovae), it is possible to carry out extremely precise measurements of the value of the Hubble constant (Treu et al. 2022; Grillo et al. 2024). Finally, the magnification produced by gravitational lenses allows us to observe and characterize objects that would otherwise be too faint to be studied.

The study of gravitational lensing benefits enormously from the angular resolution and optical stability offered by space telescopes. In particular, new generation space telescopes such as Euclid and the *James Webb Space Telescope* (JWST) are formidable tools for studying gravitational lensing. These telescopes, at the same time, are already producing a stream of data whose interpretation poses nontrivial difficulties and chal-

lenges from a computational point of view. In particular, just the modeling of multiple point-image systems in lenses made up of galaxy clusters requires performing Bayesian inference with many tens or hundreds of parameters. For example, the lens modeling of a complex system such as the galaxy cluster MACS J0416.1–2403, including 237 spectroscopically confirmed multiple images, requires several weeks of computational time on a highly parallel workstation (Bergamini et al. 2023b). When the same operation is carried out on extended sources in galaxy clusters, the complexity of the system is beyond the capacity of the currently available strong lensing codes, unless simplifications are used which severely limit the reliability of the results obtained.

Added to these technical difficulties is a question that, from a statistical point of view, is nontrivial. Several studies have shown that, even in ideal cases (identical data, relatively simple systems) the results of strong lensing analyses in galaxy clusters carried out by different researchers can produce rather different results. The problem concerns the mass estimate to a limited extent, provided the model is based on spectroscopic measurements of several image families (Grillo et al. 2015; Caminha et al. 2016; Johnson & Sharon 2016), but instead has a notable impact on other parameters such as the magnification of the images (Priewe et al. 2017). These uncertainties are typically associated with larger-than-expected scatters between the predicted and observed image positions, and are often attributed to the complexity of the lensing system, to the presence of substructures, or to the presence of perturbers along the line of sight (Priewe et al. 2017). They also represent a severe limitation to the use of strong gravitational lensing analyses for cosmological studies.

Many of the discrepancies observed in the analyses of strong lensing systems from different authors can be attributed to the different choices made in the modeling of the lens system (in addition to further sources of uncertainty, such as the associations of multiple images belonging to the same family). Since many

of the available codes are not able to evaluate the adequacy of different models of a complex system such as a galaxy cluster in an effective and statistically robust way, it is generally difficult to discriminate the various models or take systematic uncertainties into account.

All these considerations suggest that there is a need for a new generation of lensing codes, capable of performing fast and accurate lens modeling of complex systems, and of performing Bayesian inference on the model parameters, and expandable to allow the inclusion of new types of measurements. In this paper, we present `Gravity.jl`, a new proprietary gravitational lensing modeling software that aims to fulfill these requirements. `Gravity.jl` is written in the Julia programming language, and is designed with speed and flexibility in mind. In this first paper of the series, we focus on the modeling of point-like and small extended sources, and we discuss the novel statistical techniques used in the code.

For this software, we decided to use the Julia programming language (Bezanson et al. 2017). Julia is a high-level, high-performance programming language for technical computing, with syntax that is familiar to users of other technical computing environments. Although a complete discussion of the features of Julia is beyond the scope of this paper, we believe that to appreciate the advantages of `Gravity.jl` it is important to understand the main features of the language. To the end user, Julia appears as an interpreted language, much like Python, and similarly to Python, it allows one to use multiple dispatch (that is, a function can accept multiple argument types). However, Julia adopts just-in-time compilation techniques (Aycock 2003): the first time a function is called with some specific parameter types, Julia compiles it to machine code, and then caches the result. This means that Julia can achieve performance comparable to that of C or Fortran while maintaining the flexibility and ease of use of an interpreted language. Julia is also designed to be easy to use for parallel and distributed computing, as well as for GPU-based computing. Most of these advantages are associated with the use of the LLVM compiler infrastructure (Lattner & Adve 2004), which allows Julia to generate efficient machine code for a wide range of architectures.

The paper is organized as follows. In Sect. 2 we present the theoretical background, with a focus on the multiplane lensing equations and on the Bayesian inference techniques used in `Gravity.jl`. In Sect. 3 we describe the various types of measurements that can be used in the code for the various image parameters. In Sects. 4 and 5 we write the forms of the likelihood function in the two possible schemes of lensing analysis. The optimizations used for the computation of the likelihood are described in Sect. 6. In Sect. 7 we describe the most important technical aspects of the code and a few of the design choices. In Sect. 8 we present a practical use of `Gravity.jl` on a galaxy-scale lens, and we compare the results with those obtained with other codes. Finally, in Sect. 9 we draw our conclusions.

## 2. Theoretical background

### 2.1. Multiplane gravitational lensing

`Gravity.jl` can perform lensing analyses of lens systems composed of multiple lensing planes at different distances (redshifts). This capability is implemented in terms of suitable distance coefficients and is based on the multiplane lensing equations described below.

As discussed in the literature (see, e.g., Seitz & Schneider 1992 and Hilbert et al. 2009), multiplane lensing equations can

be written iteratively, essentially following backward the light path from the observer to the source. A light ray, during his path, is subject to many deflections at its intersection with the various lensing planes. These deflections are often described in the literature in terms of the reduced deflection angle  $\alpha_i = d_{i_s} \hat{\alpha}_i / d_s$ , where  $d_{i_s}$  (respectively  $d_s$ ) is the distance between the  $i$ -th lens plane and the source (respectively, the observer and the source), and  $\hat{\alpha}_i$  is the true deflection angle at the  $i$ -th lensing plane. The last quantity is actually the physical deflection and depends solely on the mass distribution at the lens plane, with no dependence on any distance.

Since `Gravity.jl` needs to deal with many lens planes and many sources at different distances, it is much more efficient to write multiplane lens equations in terms of  $\hat{\alpha}$  (rather than  $\alpha$ , as is done usually). To this purpose, let us call  $x_i$  the angular position of the intersection of the light path with the  $i$ -th lensing plane, as seen from the observer, and  $\xi_i$  the corresponding position in the lensing plane in comoving coordinates (see Fig. 1). We have then  $x_i = \xi_i / d_i$ , and  $x_1 \equiv \theta$  corresponds to the angular position of the image as seen from the observer. We call  $\delta_i$  the vector denoting the intersection of the extension of the  $i$  light path segment (that is, the path that connects the plane  $L_{i-1}$  with the plane  $L_i$ ) with the plane containing the observer  $L_0 \equiv \mathbf{O}$ . By definition, we have  $\delta_1 = 0$ . We find then

$$\delta_{i+1} = \delta_i + d_i \hat{\alpha}_i(x_i), \quad x_{i+1} = x_i - \rho_i \delta_{i+1}. \quad (1)$$

Here  $\rho_i = d_{i,i+1} / d_i$  is the ratio of the distance between the  $i$ -th plane and the next  $(i+1)$ -th plane and the distance of the  $i$ -th plane to the observer. We again note that all distances here and below are taken to be comoving transverse cosmological distances, rather than angular-diameter distances as usually done: since distance ratios are involved, this distinction is important only for the computation of the time delay below.

The advantage of using this approach is twofold. On the one hand, the computation of the deflection angles  $\hat{\alpha}_i$  can be done in a way that is independent of the distances, and therefore one can focus on the physical properties of the specific lens (instead of a combination of physical parameters and cosmological distances). Additionally, in case the distance of a lens or source plane is taken as a free parameter, the code needs to recompute just two (if the plane is the first or the last) or three distances (in the other cases), instead of a plethora of distances that would be needed if the deflection angles were computed in terms of  $\alpha$ . Finally, when the cosmological model is not known, the computation scheme used in `Gravity.jl` reduces the number of cosmological distances to compute at each change of the cosmological parameters: in the case of Fig. 1, for example, one would need to compute 7 distances, instead of 10.

The differential of previous equations gives the Jacobian matrix of the lensing equation (we note that in the case of multiplane lensing the Jacobian matrix is often not symmetric). We define

$$\Delta_1 = \begin{pmatrix} 0 & 0 \\ 0 & 0 \end{pmatrix}, \quad A_1 = \begin{pmatrix} 1 & 0 \\ 0 & 1 \end{pmatrix} \quad (2)$$

as the null and identity matrices. We then have

$$\Delta_{i+1} = \Delta_i + d_i \frac{\partial \hat{\alpha}_i(x_i)}{\partial x_i} A_i, \quad A_{i+1} = A_i - \rho_i \Delta_{i+1}. \quad (3)$$

Finally, the time delay expression can be computed as

$$T = \frac{1}{c} \sum_i \frac{1}{2} \rho_i \delta_{i+1}^2 - d_i \psi_i(x_i), \quad (4)$$

where  $\psi_i(x_i)$  is the Fermat's potential of the  $i$ -th lens plane computed at the angular position  $x_i$ .

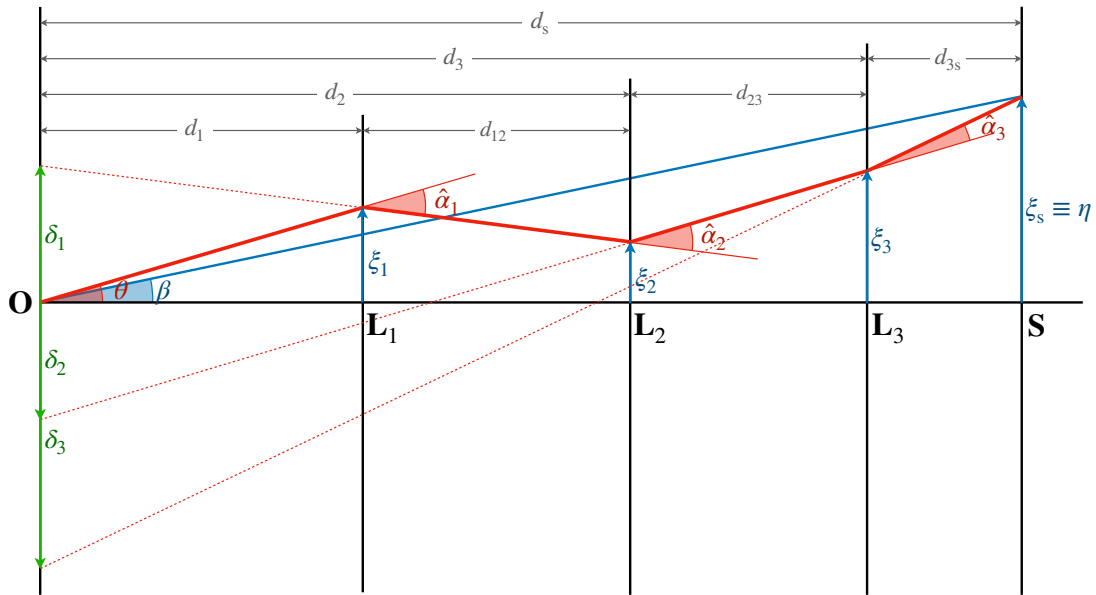


**Fig. 1.** Schematic representation of a gravitational lens system. The observer is at the left, the source at the right. The lens is composed of multiple lensing planes,  $L_i$ . A light ray (red) originating from the source plane  $S$  is deflected by the lensing planes and the associated image is formed at the observer's position along the direction  $\theta$ . The blue line in the direction  $\beta$  is the position that the source would have in the absence of lensing. The deflection angles  $\hat{\alpha}_i$  are computed at the angular positions  $x_i$  of the images. All distances needed for the computation of the relation between  $\theta$  and  $\beta$  are marked at the top of the figure.

## 2.2. Bayesian inference

Bayes' theorem (see, e.g., MacKay 2003) is at the base of the inference approach adopted in `Gravity.jl`. In its standard form, it is used to compute the probability of a set of parameters  $x$  of a model  $M$  given the (observational) data  $D$ . It can be written as

$$P(x | D, M) = \frac{P(D | x, M)P(x | M)}{P(D | M)}. \quad (5)$$

The quantity  $P(x | D, M)$  is posterior distribution of  $x$  given  $D$ , and is generally the final result we are interested in. It depends on  $P(D | x, M)$ , that is, the likelihood of the data given the parameters, and on  $P(x | M)$ , the so-called the prior distribution of the parameters. The likelihood generally encapsulates both the physical model (in our case, a multiplane lensing system) and the statistical properties of the measurements. The prior, instead, is a description of our beliefs on the parameters  $x$ , and it plays a critical role in Bayesian statistics. It should be fixed before looking at the data and should for no reason be influenced by the data. The prior is often the most controversial aspect of Bayesian statistics, and it is often the source of criticism of the Bayesian approach. In fact, the need to specify a (proper) prior is a guarantee of reproducibility of statistical inferences, as people using the same model and assuming the same prior distribution reach the same conclusions. It is important also to distinguish between the choice of a prior for the unknown model parameters, and some initial guess that one might make for the same parameters. We see below how `Gravity.jl` helps to distinguish these two concepts.

The quantity  $P(D | M)$ , often called the evidence, can be expressed as a marginalized likelihood:

$$P(D | M) = \int P(D | x', M)P(x' | M) dx', \quad (6)$$

where the integral is carried out over the relevant domain of the parameters  $x$ . The evidence is a normalization factor that ensures

that the posterior is a proper probability distribution. Its computation requires the use of a proper, normalized prior:

$$\int P(x' | M) dx' = 1. \quad (7)$$

It is usually very difficult to compute the evidence analytically, and it is often ignored in practice. It is, however, the single most important quantity, and it has a key role in the assessment of the goodness of a model in the Bayesian framework. Specifically, suppose that one wishes to evaluate  $P(M | D)$ , that is, the probability that the model  $M$  is correct, given the data  $D$ . Using Bayes' theorem, we can express this probability in terms of the evidence  $P(D | M)$ :

$$P(M | D) = \frac{P(D | M)P(M)}{P(D)}. \quad (8)$$

In this expression  $P(M)$  is a prior over  $M$ , that is, our belief that  $M$  is the correct model before looking at the data. The normalizing term  $P(D)$  is often unknown: to compute it, one would need to marginalize over all possible models, which is generally impossible. This prevents us from estimating  $P(M | D)$ , but not the ratio  $P(M | D)/P(\tilde{M} | D)$ , where  $\tilde{M}$  is an alternate model:

$$\frac{P(M | D)}{P(\tilde{M} | D)} = \frac{P(D | M) P(M)}{P(D | \tilde{M}) P(\tilde{M})}. \quad (9)$$

For this reason, in `Gravity.jl` we provide various tools to evaluate the evidence.

### 2.2.1. Prior and initial guesses

In `Gravity.jl`, we distinguish among several probability distributions:

*Prior.* It is a description of our beliefs on the model parameters, and it is used to compute the posterior distribution

through Bayes' theorem. This distribution should be fixed before looking at the data, and should not be influenced by the data. The prior should be normalized to unity as described in Eq. (7).

*Reference distribution.* Often, the algorithms used to investigate the posterior (generally based on a sampling of the posterior through Markov chain Monte Carlo techniques), require one or more initial guesses of the parameters. For example, algorithms such as Metropolis-Hasting or ensemble samplers (such as the affine-invariant sampler of Goodman & Weare 2010) require a set of initial guesses to start the sampling. These initial guesses can, but do not need to be, generated using the prior distribution: they are just a set of points in the parameter space where the sampler starts its exploration, and as such one can tailor them using the data (while, as stressed above, the prior should never make use of the data). In `Gravity.jl`, we distinguish strictly between the prior, and the distribution used to generalize the initial guesses, which we call the reference distribution.

*Posterior.* The posterior distribution of the model parameters. This distribution is the result of the application of Bayes' theorem to the prior and the likelihood. It is our belief on the model parameters after updated according to the data.

A typical use of these distributions is the following. In a first step, one might perform an initial, simplified analysis of a lens system, for example using a source-plane analysis (see below Sect. 5). For this analysis, one would set a prior distribution over the lens parameters, and use it to compute the posterior distribution. This posterior distribution can then be used to build the reference distribution, which is used to generate the initial guesses for a more complex image-plane analysis. Since the image-plane analysis makes use of additional source parameters, the reference distribution needs to be complemented with educated guesses of the source parameter distribution. Finally, this reference distribution, together with an image-plane prior, can be used to start the sampling of the final image-plane posterior distribution of the system. Although all these steps are common practice in strong gravitational lensing, they are implemented in `Gravity.jl` in a way that is as transparent as possible to the user and that strictly satisfies the requirements of Bayesian statistics.

## 2.2.2. A note on marginalization

When performing a Bayesian analysis of a complex system, we are often uninterested in a set of nuisance parameters that are needed in the modeling of the problem. A relevant example in our context is the case of source parameters in the modeling of a gravitational lens system.

In general, we can consider the likelihood associated with a gravitational lens system as formed by (at least) two sets of parameters: source parameters  $S$  (in the simpler case, the positions of all sources; in more complicated cases also their luminosities and shapes) and lens parameters  $L$ . In more complex case we might have more parameters, for example, associated with the cosmological model, but for simplicity in this discussion we ignore these cases.

Let us call  $D$  the data obtained (for example  $D = \{\hat{\theta}_n\}$  if we limit our analysis to the image positions). We write the likelihood, that is, the conditional probability of the data given the parameters, as  $P(D | S, L)$ . This quantity is then used in Bayes'

theorem so that we have

$$\begin{aligned} P(L | D) &= \int P(S, L | D) dS \\ &= \frac{P(L) \int dS P(S) P(D | S, L)}{\int dL' P(L') \int dS' P(D | S', L') P(S')} . \end{aligned} \quad (10)$$

As a result, if we write the conditional distribution  $P(D | L)$  as a marginalization over  $S$  of the full likelihood,

$$P(D | L) = \int P(D | S, L) P(S) dS , \quad (11)$$

we see that we can recover the usual form of Bayes' theorem

$$P(L | D) = \frac{P(D | L) P(L)}{\int P(D | L') P(L') dL'} . \quad (12)$$

In a sense, this marginalization corresponds to the computation of a partial evidence over the source position. The same result can be obtained by considering the definition of the conditional probability:

$$\begin{aligned} P(D | L) &= \frac{P(D, L)}{P(L)} = \frac{\int P(D, L | S) P(S) dS}{P(L)} \\ &= \int \frac{P(D, L | S)}{P(L)} P(S) dS = \int P(D | S, L) P(S) dS . \end{aligned} \quad (13)$$

Therefore, it is sensible to compute this marginalized conditional distribution. This can be done by adopting the technique described below in the paper.

## 2.2.3. Conjugate priors

It is sensible to assume that the measurements of the parameters characterizing our point-images, such as their position, their luminosity, or their shape, follow simple probability distributions. For example, position measurements can be taken to be distributed as bi-variate Gaussian. In these situations, with a suitable choice of the prior (using the so-called conjugate prior), we can make sure that the posterior belongs to the same family of the prior. This greatly simplifies the calculations and allows us to compute analytically the evidence required, as explained below.

## 3. Measurements

`Gravity.jl` is designed to work with a variety of measurements. In this section we describe the various types of measurements that can be used in the code for the various image parameters. We stress that, since in this paper we essentially focus on the modeling of point-like sources (with possible extensions such as luminosity and time delay measurements), we do not need to consider here the effects of the point-spread function (PSF) of the telescope. This effect is instead crucial for the study of extended sources, and will be discussed in a future paper.

### 3.1. Point-like sources

Image measurements are at the core of any lensing inversion. In `Gravity.jl` we assume everywhere that point-like image measurements have normal (Gaussian) errors: more precisely, we write the probability of observing an image at the position  $\theta$  given that its true position is  $\theta$  as a bivariate normal distribution

with a given known precision matrix  $\Theta$  (this matrix is the inverse of the covariance matrix, a  $2 \times 2$  symmetric matrix representing the measurement errors):

$$P(\hat{\theta} | \theta) = \sqrt{\frac{|\Theta|}{2\pi}} \exp\left[-\frac{1}{2}(\hat{\theta} - \theta)^T \Theta (\hat{\theta} - \theta)\right]. \quad (14)$$

We also assume that all image measurements are independent: as a result, when computing the joined probability to observe a set of images  $\{\hat{\theta}_i\}$  given the corresponding predictions  $\{\theta_i\}$ , we can just write

$$P(\{\hat{\theta}_i\} | \{\theta_i\}) = \prod_{i=1}^l \sqrt{\frac{|\Theta_i|}{2\pi}} \exp\left[-\frac{1}{2}(\hat{\theta}_i - \theta_i)^T \Theta_i (\hat{\theta}_i - \theta_i)\right]. \quad (15)$$

This is effectively the likelihood generally used in the code.

### 3.2. Luminous sources

In case where we also measure the images' magnitudes  $\{\hat{m}_i\}$  and their associated inverse variances  $\{\lambda_i\}$  we can easily add the related constraints to the previous equations. The likelihood associated with the magnitudes is simply

$$P(\{\hat{m}_i\} | \{m_i\}) = \prod_{i=1}^l \sqrt{\frac{\lambda_i}{2\pi}} \exp\left[-\frac{1}{2}\lambda_i(\hat{m}_i - m_i)\right]. \quad (16)$$

The observed magnitudes are related to the original (unlensed) one  $M$  through the relation

$$m_i = M - 2.5 \log_{10}|A_i^{-1}| \equiv M - LM_i, \quad (17)$$

where we have called  $LM_i \equiv 2.5 \log_{10}|A_i^{-1}|$  the lensing modulus, a quantity that indicates the change in magnitude associated with the lensing magnification. With this definition, we can write the likelihood as

$$P(\{\hat{m}_i\} | M) = \prod_{i=1}^l \sqrt{\frac{\lambda_i}{2\pi}} \exp\left[-\frac{1}{2}\lambda_i(\hat{m}_i + LM_i - M)^2\right]. \quad (18)$$

### 3.3. Elliptical sources

As a third source type, we consider sources with an elliptical profile. These sources can be characterized using the quadrupole moment of their light distribution: for a source with semi-axes  $a$  and  $b$  and position angle  $\varphi$  counted clockwise from the top (north to west in astronomical sense), the quadrupole moment is

$$Q = \begin{pmatrix} a^2 \sin^2 \varphi + b^2 \cos^2 \varphi & (a^2 - b^2) \sin \varphi \cos \varphi \\ (a^2 - b^2) \sin \varphi \cos \varphi & a^2 \cos^2 \varphi + b^2 \sin^2 \varphi \end{pmatrix}. \quad (19)$$

We note how the quadrupole moment is a symmetric and positive-definite matrix. We take quadrupole moment measurements to be unaffected by the PSF (or, more realistic, we assume that the effects of the PSF have been removed). We also assume that they are distributed according to a Wishart distribution (see, e.g., Livan et al. 2018), with probability density function given by

$$P(\hat{Q} | \mathbf{W}, \nu) = \frac{|\mathbf{W}|^{\nu/2}}{2^{\nu p/2} \Gamma_p(\nu/2)} |\hat{Q}|^{(\nu-p-1)/2} \exp[-\text{tr}(\mathbf{W}\hat{Q})/2], \quad (20)$$

where  $p = 2$  is the dimensionality of the space,  $\nu > p + 1$  is a real number, and  $\mathbf{W}$  is a symmetric, positive definite matrix. The

equation above also uses  $\Gamma_p$ , the multivariate Gamma function. For the specific case  $p = 2$  we have

$$\Gamma_2(\nu/2) = \pi 2^{2-\nu} \Gamma(\nu - 1). \quad (21)$$

Therefore, for  $p = 2$  the probability distribution function simplifies into

$$P(\hat{Q} | \mathbf{W}, \nu) = \frac{|\mathbf{W}|^{\nu/2}}{4\pi \Gamma(\nu - 1)} |\hat{Q}|^{(\nu-3)/2} \exp[-\text{tr}(\mathbf{W}\hat{Q})/2]. \quad (22)$$

The mode of this distribution is  $(\nu - p - 1)\mathbf{W}^{-1} = (\nu - 3)\mathbf{W}^{-1}$ , while the average is  $\nu\mathbf{W}^{-1}$ . As usual, we assume that all measurements are independent, so that the joint distribution for various elliptical measurements can be obtained as a product of terms such as the one written above. We note that here we use the canonical parameter  $\mathbf{W}$  instead of the more usual choice  $\mathbf{V} \equiv \mathbf{W}^{-1}$ .

A quadrupole measurement is generally given in terms of a measured shape, often given in terms of the semi-axes ( $a$  and  $b$ ) and of a position angle ( $\theta$ ), together with their associated errors ( $\sigma_a, \sigma_b, \sigma_\theta$ ). A quadrupole moment  $\hat{Q}$  can be easily built using the set  $\{a, b, \theta\}$  from the equations above. We see below how we model the intrinsic quadrupole of a source and its relation to the  $\mathbf{W}$  matrix. Regarding  $\nu$ , it is easy to show that, to first order, one has

$$\frac{\sigma_a}{a} = \frac{\sigma_b}{b} = \frac{2}{\sqrt{\nu}}, \quad (23)$$

where  $\sigma_a$  and  $\sigma_b$  are the measurement uncertainties on the semi-axes  $a$  and  $b$ .

### 3.4. Time delays

In some cases, we have at our disposal time delays for the multiple images of a point source, and we want to take advantage of this information. This is particularly useful for cosmological measurements, in particular the ones related to the Hubble's constant.

The situation here, from a statistical point of view, is virtually identical to the case of magnitude measurements. Specifically, suppose we measure the images' time delays  $\{\hat{t}_i\}$  and their associated inverse variances  $\tau_i$ . We note that, typically, time delays are given as differences in arrival time concerning a given source. In `Gravity.jl` we assume that all images of a given source are given a time delay: this, in practice, means that one usually sets the measured time delay of the reference image to zero with a very small error (i.e., a very large precision  $\tau_i$ ).

The computation of time delays requires the knowledge of Fermat's potential, which for many lens models is a relatively expensive operation. From a statistical point of view, however, all equations for time delay measurements reflect the ones for magnitude measurements. Throughout the code we assume that the time delay values  $\hat{t}_i$  are given with respect to a reference event: for example, we could set the time delay of a reference image to zero, and measure the time delays of the other images with respect to this reference. The likelihood for the time delays can then be written as

$$P(\{\hat{t}_i\} | \{t_i\}) = \prod_{i=1}^l \sqrt{\frac{\tau_i}{2\pi}} \exp\left[-\frac{1}{2}\tau_i(\hat{t}_i - t_i)\right], \quad (24)$$

with the expected time delays  $\{t_i\}$  written as

$$t_i = T + T_i. \quad (25)$$

Here we have called  $T_i$  the time delay function for the  $i$ -th image, and  $T$  the reference time for the source.

### 3.5. Log-likelihoods

Generally, we are dealing with the log-likelihood, which therefore can be written as

$$\log P(\{\hat{\theta}_i\} | \{\theta_i\}) = \sum_{i=1}^I \left[ \frac{1}{2} \log \left| \frac{\mathbf{\Theta}_i}{2\pi} \right| - \frac{1}{2} (\hat{\theta}_i - \theta_i)^T \mathbf{\Theta}_i (\hat{\theta}_i - \theta_i) \right], \quad (26)$$

for the positions,

$$\log P(\{\hat{m}_i\} | M) = \sum_{i=1}^I \left[ \frac{1}{2} \log \frac{\lambda_i}{2\pi} - \frac{1}{2} \lambda_i (\hat{m}_i + LM_i - M)^2 \right], \quad (27)$$

for the magnitudes (and similarly for the time delays), and

$$\log P(\{\hat{Q}_i\} | \{\mathbf{W}_i\}, \{v_i\}) = \sum_{i=1}^I \left[ \frac{v_i}{2} \log |\mathbf{W}_i| - \log [4\pi \Gamma(v_i - 1)] + \frac{v_i - 3}{2} \log |\hat{Q}_i| - \frac{1}{2} \text{tr}(\mathbf{W}_i \hat{Q}_i) \right], \quad (28)$$

for the quadrupole moments.

In a maximum-likelihood approach, in many cases one can safely ignore the normalizing constants in the expressions above, corresponding in all cases to the first two terms inside the summations, as their values typically depend only on the measurement errors associated with each observed image, and not on the predicted images. In a Bayesian approach, instead, the normalizing constants can be relevant, especially when a marginalization over the source parameters is performed, or when one wishes to compare different lensing models.

When dealing with these expressions, we need to consider various issues

1. How are the predicted images  $\{\theta_i\}$  computed?
2. How do we associate an observed image to the corresponding predicted one?
3. What do we do if the number of predicted images differs from the number of observed ones?

We consider all these issues below.

## 4. Image-plane likelihood

The most straightforward way to compute the likelihood of a lens model is to include explicitly the source parameters (positions, magnitudes, quadrupole moments...) in the model, and to perform an inversion of the lens mapping and associate the counter-images of a given source. All these operations, as noted above, are nontrivial and time consuming. For this reason, usually, an image-plane optimization is carried out only after an approximate lens model has been found using a source-plane optimization (see below Sect. 5).

In principle, once the counter-images of a given source have been found, the computation of the image-plane likelihood is a mere application of the equations written in the previous section. In practice, things are a little more complicated because (1) the inversion of the lens equation might produce too many or too few predicted images, and (2) the predicted images might not be associated with the observed ones in a one-to-one way. We consider these issues below. In the following we reserve the subscript  $i \in \{1, \dots, I\}$  to indicate the observed images and the subscript  $p \in \{1, \dots, P\}$  for the predicted images from a given source.

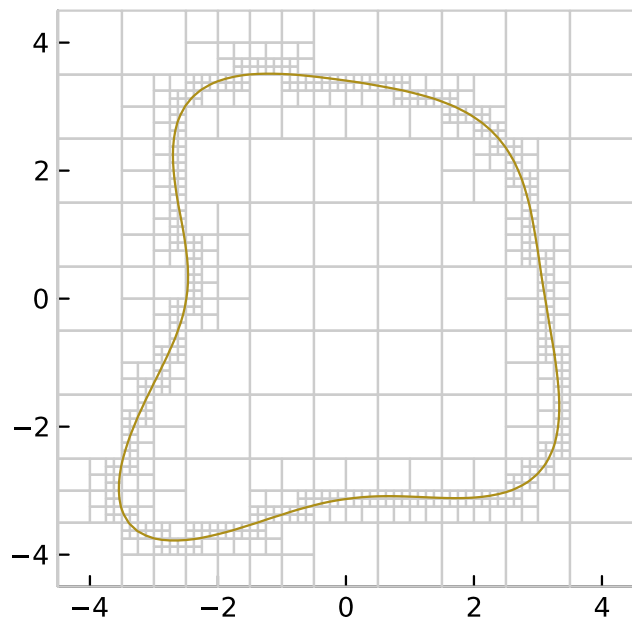


Fig. 2. Example of grid with an order=3 refinement near a critical curve.

### 4.1. Inversion of the lens equation

The inversion of the lens equation, that is, the discovery of the image positions associated with a given source position, plays a central role in the image-plane likelihood. This task is generally carried out using a nonlinear equation solver. Many nonlinear equation solvers are known, but in *Gravity.jl* we have decided to use the simplest one, Newton–Raphson’s method.

Newton’s method, like any iterative method, requires a starting guess of the solution. When we have already a good approximation of the lens model, we can generally safely use the positions of the observed images as starting points of the method. The convergence of the lens inversion method is in these cases generally very fast, unless the Jacobian of the lens equation is not well-behaved (this can happen for sources on top of critical curves with formally infinite magnification, or for lens models with singularities).

In case we do not have a good lens model, or in case we wish to find new solutions of the lens equations (for example, to find possible counter-images), we can use a suitable grid and map all grid cells into the source plane using the lens equation. We can then identify the cells that, when mapped in the source plane, enclose the source position, and use their centers (or better, the inverse of the source position using a linear approximation of the lens equation) as guesses for the solution. If the grid is suitable built, this technique generally ensures that we find all possible solutions of the lens equation, at the expense of a much higher computational complexity. This task, which can be easily parallelized, is optionally associated with a hierarchical binary refinement of the grid cell near critical lines, observed images, or centers of the lens profiles, to ensure as much as possible that all possible solutions are found. Figure 2 shows an example of such a grid refinement.

Our grid algorithm has been designed to be as general and as robust as possible. Critical lines are refined using a simple criterion based on the sign of the determinant of the Jacobian at the vertices of each cell (following a prescription also adopted by Jullo et al. 2007): When the sign changes between the two

vertices of a cell side, the cell is refined. The algorithm proceeds then recursively, refining the cells that are found to be on the critical lines. We note that during this refinement procedure, it might happen that an unrefined cell is found to be on a critical line: in this case, the cell is refined as well. This latter point is important, as it guarantees that critical lines are always resolved with the desired accuracy and also avoid artifacts when drawing critical lines (see, e.g., Fig. A2 of Jullo et al. 2007 or Fig. 1.1 of the manual of Glafic 2, Oguri 2010, 2021).

## 4.2. Image positions

In the simplest case, the log-likelihood for a given family of predicted images includes only the image positions. This case, considered here, shows already several interesting features.

### 4.2.1. Direct association

If, somehow, we have sorted out the predicted images so that each of them is associated with the corresponding observed image (which necessarily implies  $I = P$ ), we can just compute the log-likelihood as

$$2 \log P(\{\hat{\theta}_i\} | \{\theta_i\}) = \sum_{i=1}^I \log \left| \frac{\mathbf{Q}_i}{2\pi} \right| - (\hat{\theta}_i - \theta_i)^T \mathbf{Q}_i (\hat{\theta}_i - \theta_i). \quad (29)$$

The log-likelihood expression above can be easily differentiated with respect to the source position  $\beta$ : taking into account again the theorem of the inverse function, we find

$$\frac{\partial \log P(\{\hat{\theta}_i\} | \{\theta_i\})}{\partial \beta} = \sum_{i=1}^I A_i^{-T} \mathbf{Q}_i (\hat{\theta}_i - \theta_i). \quad (30)$$

This quantity can be useful when performing a likelihood maximization over the source position, or when using Monte Carlo techniques that require the derivatives of the posterior (such as Hamiltonian Monte Carlo).

### 4.2.2. Best match

In many cases, we cannot associate directly one observed image with one predicted image. This can happen, for example, when the lens model is not accurate enough, or when the source is very close to a critical curve. In these cases, we might decide to find the best association between the observed and predicted images, and use this association to compute the likelihood.

Let us call  $\sigma$  the permutation that associates each observed image to one predicted image. We can then write the log-likelihood as

$$2 \log P(\{\hat{\theta}_i\} | \{\theta_p\}, \sigma) = \sum_{i=1}^I \log \left| \frac{\mathbf{Q}_i}{2\pi} \right| - (\hat{\theta}_i - \theta_{\sigma(i)})^T \mathbf{Q}_i (\hat{\theta}_i - \theta_{\sigma(i)}), \quad (31)$$

We use different subscripts for the images and predictions because we have, in general, different numbers of them. The procedure finds the permutation  $\sigma$  that maximizes the expression above and returns the maximum value found, together with the Jacobian with respect to the source position.

The exact meaning of ‘‘permutation’’ here depends on a specific choice:

- We might use for  $\sigma$  permutations with repetitions: this way, each observed image can be matched to each predicted one with no restriction, so that two observed images could be in principle associated with the same predicted one. This way we have  $P^I$  different permutations. In practice, finding the best permutation is very simple: we just compute all possible sum terms above and take the best ones for each source. Thus, essentially, for each observed image we take the closest predicted image in terms of Mahalanobis distance (Mahalanobis 1936).
- Alternatively, we might use permutations without repetitions: in this case one predicted image can be associated with one observed image at most, resulting in  ${}^P P_I = P!/(P-I)!$  possible permutations. In this case, finding the best permutation is more complicated, as we need to check that we do not have repetitions in the best solution. The strategy we adopt to find the best  $\sigma$  is to try the same technique as in the case of permutations with repetition, and check if we have repetitions in the best solution: if we do not, we take this solution; if we do, we loop over the (possibly large) number of permutations and take the best one. This choice requires that the predicted images are at least as numerous as the observed ones, so that  $P \geq I$ . This is potentially problematic, as it might prevent a convergence if the lensing model is far from a realistic configuration.

### 4.2.3. Marginalization over all matches

Looking again at the previous subsection, we can easily recognize that the permutation  $\sigma$  is a nuisance parameter: we are not really interested in knowing its value, as we merely use it to compute the likelihood. In a more correct Bayesian approach, we should therefore marginalize over all accepted permutations  $\Sigma$  and write

$$P(\{\hat{\theta}_i\} | \{\theta_p\}) = \sum_{\sigma \in \Sigma} P(\{\hat{\theta}_i\} | \{\theta_{\sigma(i)}\}, \sigma) P(\sigma) = \frac{1}{|\Sigma|} \sum_{\sigma \in \Sigma} \prod_{i=1}^I P(\hat{\theta}_i | \theta_{\sigma(i)}). \quad (32)$$

Here we have assumed that all permutations have the same probability,  $P(\sigma) = 1/|\Sigma|$  where  $|\Sigma|$  is the number of allowed permutations: that is,  $|\Sigma| = P^I$  for permutations with repetitions, or  $|\Sigma| = P!/(P-I)!$  for  $I$ -permutations (without repetitions).

Computationally, this expression can be evaluated in two different ways depending on the permutation type. In the case of permutations with repetitions we simply have

$$P(\{\hat{\theta}_i\} | \{\theta_p\}) = \frac{1}{|\Sigma|} \prod_{i=1}^I \sum_{p=1}^P P(\hat{\theta}_i | \theta_p). \quad (33)$$

This expression, written in terms of log-quantities, becomes

$$\log P(\{\hat{\theta}_i\} | \{\theta_p\}) = -\log |\Sigma| + \sum_{i=1}^I \bigwedge_{p=1}^P \log P(\hat{\theta}_i | \theta_p), \quad (34)$$

where  $\bigwedge_p$  denotes the LogSumExp (see, e.g., Blanchard et al. 2020) operation over  $p$ . Its gradient is given by

$$\frac{\partial \log P(\{\hat{\theta}_i\} | \{\theta_p\})}{\partial \beta} = \sum_{i=1}^I \sum_{p=1}^P \text{softmax}_p[\log P(\hat{\theta}_i | \theta_p)] \cdot A_i^{-T} \mathbf{Q}_i (\hat{\theta}_i - \theta_p), \quad (35)$$

where softmax is the softmax function:

$$\text{softmax}_p(x_p) = \frac{\exp x_p}{\sum_{p'} \exp x_{p'}}. \quad (36)$$

In the case of permutations without repetitions, instead, we cannot perform the simplification above, and we have therefore

$$\log P(\{\hat{\theta}_i\} | \{\theta_p\}) = -\log |\Sigma| + \sum_{\sigma} \left[ \sum_{i=1}^I \log P(\hat{\theta}_i | \theta_{\sigma(i)}) \right]. \quad (37)$$

The gradient of this expression is

$$\frac{\partial \log P(\{\hat{\theta}_i\} | \{\theta_p\})}{\partial \beta} = \text{softmax}_{\sigma} \left[ \sum_{i=1}^I \log P(\hat{\theta}_i | \theta_p) \right] \cdot \sum_{i=1}^I A_i^{-T} \Theta_i (\hat{\theta}_i - \theta_{\sigma(i)}), \quad (38)$$

Finally, we note that the use of the normalization  $1/|\Sigma|$  above introduces, effectively, a factor that penalizes cases where we have many images predicted and only a few images observed. This is very sensible and shows that the approach followed here naturally encapsulates a penalty factor for unobserved images.

#### 4.3. Magnitudes

We now consider the case of luminous image measurements and provide analytic expressions for the (logarithmic) likelihood associated with the magnitude measurements. We stress that, similarly to other source properties described below, the use of individual measurements, instead of derived quantities (such as, for example, the flux ratios) allows us to work with statistically independent quantities. We note also that since the Jacobian of the lens mapping is already used to compute the magnification factor (lens modules), we cannot provide any derivative of the likelihood for magnitudes without higher order derivatives of the lens mapping.

If we suppose that the intrinsic (unlensed) magnitude  $M$  is a given parameter, the generalization of the results of the previous subsection is trivial: essentially, we just need to consider additional terms associated with the magnitude measurements. For example, the result obtained for the direct match is

$$2 \log P(\{\hat{\theta}_i\}, \{\hat{m}_i\} | \{\theta_i\}, M) = \sum_{i=1}^I \log \left| \frac{\Theta_i}{2\pi} \right| - (\hat{\theta}_i - \theta_i)^T \Theta_i (\hat{\theta}_i - \theta_i) + \log \frac{\lambda_i}{2\pi} - \lambda_i (\hat{m}_i + LM_i - M)^2. \quad (39)$$

The other methods are easily generalized.

The fact that the source magnitude  $M$  enters the log-likelihood in a simple way allows us to perform an important simplification and to avoid the use of an explicit parameter for this quantity. We defer this discussion to Sect. 6.1.

#### 4.4. Quadrupole moments

Sources with quadrupole measurements have a log-likelihood of the form

$$2 \log P(\{\hat{\theta}_i\}, \{\hat{m}_i\}, \{\hat{Q}_i\} | \{\theta_i\}, M, \mathbf{S}, \{\nu_i\}) = \sum_{i=1}^I \left[ \log \left| \frac{\Theta_i}{2\pi} \right| - (\hat{\theta}_i - \theta_i)^T \Theta_i (\hat{\theta}_i - \theta_i) + \log \frac{\lambda_i}{2\pi} - \lambda_i (\hat{m}_i + LM_i - M)^2 + \frac{\nu_i}{2} \log |\nu_i A_i^T \mathbf{S} A_i| - \log [4\pi \Gamma(\nu_i - 1)] + \frac{\nu_i - 3}{2} \log |\hat{Q}_i| - \nu_i \text{tr}(A_i^T \mathbf{S} A_i \hat{Q}_i) \right], \quad (40)$$

where we have called  $\mathbf{S}$  the inverse of the source quadrupole and where we have split in each line the contribution from the three different measurements (positions, magnitudes, and quadrupole moments).

For this kind of source, we can apply arguments similar to the ones discussed above. In particular, if we keep  $M$  and  $\mathbf{S}$  as free parameters, the computation of the log-likelihood proceeds as for point-sources, with the additional terms associated with the magnitudes and quadrupole moments.

#### 4.5. Time delay measurements

For point-sources with associated time delays we can define a log-likelihood function following closely what is done for luminous image measurements. The equations, from a mathematical point of view, are identical, and we also have again the possibility of performing a marginalization over the source time  $T$ .

### 5. Source-plane likelihood

#### 5.1. Positions

The easiest way to evaluate the likelihood above is to avoid, as much as possible, the computation of the predicted images  $\{\theta_i\}$ . This task requires the inversion of the nonlinear lens mapping, something nontrivial and rather time consuming.

The approach uses a simple idea. Consider the lens equation

$$\beta = f(\theta). \quad (41)$$

If  $\beta$  is a regular value, this nonlinear equation admits local inverses that we call  $f_i^{-1}$ : that is, each predicted image  $\theta_i$  of the  $\beta$  is given by

$$\theta_i = f_i^{-1}(\beta). \quad (42)$$

We can perform a Taylor expansion to first order of these equations around  $f(\hat{\theta}_i) \equiv \hat{\beta}_i$  to obtain

$$\theta_i = f_i^{-1}(\beta) \approx f_i^{-1}(\hat{\beta}_i) + \frac{\partial f_i^{-1}}{\partial \beta} \Big|_{\hat{\beta}_i} (\beta - \hat{\beta}_i) = \hat{\theta}_i + \frac{\partial f_i^{-1}}{\partial \beta} \Big|_{\hat{\beta}_i} (\beta - \hat{\beta}_i). \quad (43)$$

From the inverse function theorem, we can write the Jacobian of the inverse  $f_i^{-1}$  evaluated at  $\hat{\beta}_i$  as the inverse of the Jacobian of  $f$  evaluated at the corresponding point,  $\hat{\theta}_i$ . We find therefore

$$\hat{\theta}_i - \theta_i = A_i^{-1}(\hat{\beta}_i - \beta), \quad (44)$$



where we have called

$$A_i = \frac{\partial f}{\partial \theta} \Big|_{\hat{\theta}_i}. \quad (45)$$

Using this approximation in the log-likelihood above we find

$$\log P(\{\hat{\theta}_i\} | \beta) = \sum_{i=1}^I \frac{1}{2} \log \left| \frac{\Theta_i}{2\pi} \right| - \frac{1}{2} (\hat{\beta}_i - \beta)^T B_i (\hat{\beta}_i - \beta), \quad (46)$$

where  $B_i \equiv A_i^{-T} \Theta_i A_i^{-1}$  is a symmetric matrix representing the  $i$ -th precision  $\Theta_i$  mapped into the source plane.

Taken as a function for  $\beta$ , this expression can be written as a bivariate Gaussian:

$$\log P(\{\hat{\theta}_i\} | \beta) = \text{const} - \frac{1}{2} (\beta - \bar{\beta})^T B (\beta - \bar{\beta}), \quad (47)$$

where the mean  $\bar{\beta}$  and the precision  $B$  are given by

$$B = \sum_{i=1}^I A_i^{-T} \Theta_i A_i^{-1} = \sum_{i=1}^I B_i, \quad (48)$$

$$\bar{\beta} = B^{-1} \sum_{i=1}^I A_i^{-T} \Theta_i A_i^{-1} \hat{\beta}_i = B^{-1} \sum_{i=1}^I B_i \hat{\beta}_i. \quad (49)$$

As a result, we can immediately write the maximum-likelihood solution (and its precision matrix) as  $\bar{\beta}$  (and  $B$ ).

In a frequentist approach, we could just substitute the maximum-likelihood solution  $\beta = \bar{\beta}$  into the likelihood and compute its maximum-likelihood value: this, in turn, could be used in an outer optimization loop, where we would change the lensing parameters until we obtain a maximum of this source-plane likelihood.

If, instead, we adopt a Bayesian approach, we should proceed as explained above and compute the marginalized likelihood over the source positions. Since the conjugate prior in our case is also a bi-variate normal distribution, we assume that  $\beta$  is distributed as

$$P(\beta | \hat{\beta}_0, B_0) = \sqrt{\left| \frac{B_0}{2\pi} \right|} \exp \left[ -\frac{1}{2} (\beta - \hat{\beta}_0)^T B_0 (\beta - \hat{\beta}_0) \right]. \quad (50)$$

Here  $\hat{\beta}_0$  and  $B_0$  are meta-parameters that describe the prior on the source position:  $\hat{\beta}_0$  is the center of the distribution, and  $B_0$  is its precision. Typically, one starts with a very loose prior, and therefore one might set  $B_0$  might be chosen as a (very) small multiple of the identity matrix.

In this approach, we apply Bayes' theorem and write the posterior distribution for  $\beta$  as

$$P(\beta | \{\hat{\theta}_i\}) = \frac{\log P(\{\hat{\theta}_i\} | \beta) P(\beta | \hat{\beta}_0, B_0)}{\int \log P(\{\hat{\theta}_i\} | \beta') P(\beta' | \hat{\beta}_0, B_0) d\beta'}. \quad (51)$$

A simple calculation then shows that the numerator of the posterior, the expression  $P(\{\hat{\theta}_i\} | \beta) P(\beta | \hat{\beta}_0, B_0)$ , taken as a function of  $\beta$  is proportional to a multivariate normal distribution with updated meta-parameters

$$B = B_0 + \sum_{i=1}^I B_i = \sum_{i=0}^I B_i, \quad (52)$$

$$\bar{\beta} = B^{-1} (B_0 \hat{\beta}_0 + B\beta) = B^{-1} \sum_{i=0}^I B_i \hat{\beta}_i. \quad (53)$$

We note how these results are formally identical to the ones found above, with the (slight) difference that the sums start at  $i = 0$  and includes, therefore, the prior meta-parameters.

The normalizing constant, that is, the denominator in the posterior distribution, is generally called the evidence or the marginalized likelihood. Its logarithm can be written as

$$2 \log E = \sum_{i=0}^I \left[ \log \left| \frac{\Theta_i}{2\pi} \right| - \hat{\beta}_i^T B_i \hat{\beta}_i \right] - \left[ \log \left| \frac{B}{2\pi} \right| - \bar{\beta}^T B_0 \bar{\beta} \right], \quad (54)$$

or, equivalently,

$$2 \log E = \sum_{i=0}^I \left[ \log \left| \frac{\Theta_i}{2\pi} \right| - (\hat{\beta}_i - \bar{\beta})^T B_i (\hat{\beta}_i - \bar{\beta}) \right] - \log \left| \frac{B}{2\pi} \right|. \quad (55)$$

We note that in these expressions we have defined  $\Theta_0 \equiv B_0$ , so to be able to include the prior normalizing constant in a way similar to the other measurements. The evidence  $E$ , in our Bayesian approach, replaces the likelihood, as it is effectively a likelihood marginalized over the source position (or, more generally, the source parameters).

In many cases, it is convenient to consider also an evidence based on a flat prior. In our notation, this corresponds to taking the limit

$$E_0 = \lim_{\Theta_0 \rightarrow 0} E \left| \frac{\Theta_0}{2\pi} \right|^{-1/2}, \quad (56)$$

that is, to the use of an improper prior  $P(\beta_0) = 1$ . The expressions obtained for  $\log E_0$  are formally identical to the expressions above for  $\log E$ , with the sums starting at  $i = 1$ . More explicitly:

$$2 \log E_0 = \sum_{i=1}^I \left[ \log \left| \frac{\Theta_i}{2\pi} \right| - \hat{\beta}_i^T A_i^{-T} \Theta_i A_i^{-1} \hat{\beta}_i \right] - \log \left| \frac{B}{2\pi} \right| + \bar{\beta}^T B \bar{\beta}, \quad (57)$$

or, equivalently,

$$2 \log E_0 = \sum_{i=1}^I \left[ \log \left| \frac{\Theta_i}{2\pi} \right| - (\hat{\beta}_i - \bar{\beta})^T A_i^{-T} \Theta_i A_i^{-1} (\hat{\beta}_i - \bar{\beta}) \right] - \log \left| \frac{B}{2\pi} \right|. \quad (58)$$

Naively, we could imagine that this expression is equivalent to a substitution of the maximum-likelihood solution  $\beta = \bar{\beta}$  inside the likelihood. This, however, is not the case: the additional term to the right,  $\log |B/2\pi|$ , is a nontrivial addition since it is influenced by the jacobian matrices of the lens-mapping equation at the observed image positions  $\{A_i\}$ , and therefore depends on the chosen lens model.<sup>1</sup>

## 5.2. Magnitudes

Luminous sources are characterized by their position and luminosity. Here, we prefer to describe them in terms of magnitudes, as this is more directly interpreted in terms of practical measurements, and because of the possible use of a specific prior (see below).

As usual, we can proceed as before and assume initially that the unknown source magnitude  $M$  has a normal (Gaussian) distribution for its prior:

$$P(M | \hat{M}_0, \lambda_0) = \sqrt{\frac{\lambda_0}{2\pi}} \exp \left[ -\frac{1}{2} \lambda_0 (\hat{M} - M_0)^2 \right]. \quad (59)$$

<sup>1</sup> The use of this marginalized likelihood is controlled in the code by the flag `bayesianfactor`.

With a calculation similar to the one discussed above, we easily find that the posterior probability distribution for the source magnitude  $M$  is a Gaussian with precision (inverse variance)

$$\lambda = \sum_{i=0}^I \lambda_i \quad (60)$$

and mean

$$\bar{M} = \lambda^{-1} \sum_{i=0}^I \lambda_i (\hat{m}_i + LM_i) = \lambda^{-1} \sum_{i=0}^I \lambda_i \hat{M}_i, \quad (61)$$

where we have called  $\hat{M}_i \equiv \hat{m}_i + LM_i$ . The corresponding evidence is

$$2 \log E = \sum_{i=0}^I \left[ \log \frac{\lambda_i}{2\pi} - \lambda_i \hat{M}_i^2 \right] - \left[ \log \frac{\lambda}{2\pi} - \lambda \bar{M}^2 \right], \quad (62)$$

or, equivalently,

$$2 \log E = \sum_{i=0}^I \left[ \log \frac{\lambda_i}{2\pi} - \lambda_i (\hat{M}_i - \bar{M})^2 \right] - \log \frac{\lambda}{2\pi}. \quad (63)$$

As before, it can be sensible to consider the case of an improper flat prior and consider the limit  $\lambda_0 \rightarrow 0$ . Again, this produces an evidence  $E_0$  which is formally identical to the expression for  $E$ , with the sum starting at  $i = 1$ .

For magnitudes, it might also be interesting to consider the improper prior

$$P(\hat{M}_0 | \alpha) \propto e^{\alpha \hat{M}_0}. \quad (64)$$

This model is justified by the number counts of distant sources, which under mild hypotheses are distributed according to an exponential law with  $\alpha = 0.6 \ln 10 \approx 1.38$ . In this case, we find

$$\lambda = \sum_{i=1}^I \lambda_i, \quad (65)$$

$$\bar{M} = \lambda^{-1} \left[ \alpha + \sum_{i=1}^I \lambda_i \hat{M}_i \right], \quad (66)$$

while the evidence under the new prior is still

$$2 \log E_\alpha = \sum_{i=1}^I \left[ \log \frac{\lambda_i}{2\pi} - \lambda_i \hat{M}_i^2 \right] - \left[ \log \frac{\lambda}{2\pi} - \lambda \bar{M}^2 \right]. \quad (67)$$

We note how  $\alpha = 0$  returns the usual expressions for a flat improper prior.

### 5.3. Quadrupole measurements

Let us call  $\mathbf{S}$  the inverse of the source quadrupole. Since  $\langle \hat{Q}_i \rangle = v_i \mathbf{W}_i^{-1}$ , and since quadrupole moments transform as rank-two tensors, we have

$$\mathbf{W}_i = v_i A_i^T \mathbf{S} A_i. \quad (68)$$

If we insert this equation in the likelihood for the quadrupole moments we find

$$\log P(\{\hat{Q}_i\} | \mathbf{S}, \{v_i\}) = \sum_{i=1}^I \left[ \frac{v_i}{2} \log |v_i A_i^T \mathbf{S} A_i| - \log [4\pi\Gamma(v_i - 1)] \right. \\ \left. + \frac{v_i - 3}{2} \log |\hat{Q}_i| - \frac{v_i}{2} \text{tr}(A_i^T \mathbf{S} A_i \hat{Q}_i) \right]. \quad (69)$$

To proceed, we now consider the prior distribution for the inverse source quadrupole  $\mathbf{S}$ . We decide to use for this quantity also as a Wishart prior, with meta-parameters  $\hat{O}_0$  and  $v_0$ :

$$\log P(\mathbf{S} | \hat{O}_0, v_0) = \frac{v_0}{2} \log |v_0 \hat{O}_0| - \log [4\pi\Gamma(v_0 - 1)] \\ + \frac{v_0 - 3}{2} \log |\mathbf{S}| - \frac{v_0}{2} \text{tr}(\hat{O}_0 \mathbf{S}). \quad (70)$$

We note that our choice for the prior of  $S$  implies that the source quadrupole has an inverse Wishart distribution (Wishart 1928) as prior. The product between the prior and the likelihood, taken as a function of  $\mathbf{S}$ , still has the same form as the prior. To show this, one can use the cyclic property of the trace and the expression for the determinant of the product of matrices. The posterior has updated meta-parameters

$$v = v_0 + \sum_{i=1}^I v_i = \sum_{i=0}^I v_i \quad (71)$$

and

$$\bar{O} = \frac{1}{v} \left[ v_0 \hat{O}_0 + \sum_{i=1}^I v_i A_i \hat{Q}_i A_i^T \right] = \frac{1}{v} \sum_{i=0}^I v_i \hat{O}_i, \quad (72)$$

where we have called  $\hat{O}_i \equiv A_i \hat{Q}_i A_i^T$ . The expression above shows that, essentially, the parameter  $\bar{O}$ , representing an estimate for the source quadrupole, is a weighted average of the measured quadrupole moments projected into the source plane, with weights  $v_i$ .

The evidence associated with the updated distribution is

$$\log E = \sum_{i=0}^I \frac{v_i}{2} \log |v_i \hat{O}_i| - \frac{v}{2} \log |v \bar{O}| \\ - \sum_{i=0}^I \log [4\pi\Gamma(v_i - 1)] + \log [4\pi\Gamma(v - 1)] \\ - \frac{3}{2} \sum_{i=1}^I \log |\hat{Q}_i|. \quad (73)$$

This expression, whose symmetry is evident, depends on the lensing model only through the first two terms, as are both functions of the set of lensing Jacobian matrices  $\{A_i\}$ . The other terms, instead, only depend on the measurements. We note also how the largest evidence is obtained when all projected quadrupole moments  $\{\hat{O}_i\}$  agree, as in this case there are no cancellation effects in the expression for  $\bar{O}$ .

As before, we can consider an uninformative improper prior characterized by  $v_0 = 0$ . In that case, the expressions above are just essentially the same, with all sums starting from  $i = 1$ .

### 5.4. Time delays

As mentioned already, the equations that describe the time delays are formally identical to the ones that describe the magnitudes. They are both scalar quantities that depend on a single scalar source parameter (the unlensed magnitude  $M$  or the reference time  $T$ ) through additive terms (the lensing modules  $LM_i$  or the time delays  $T_i$ ). Moreover, for the measurements of both quantities, we assume simple normal distributions.

**Table 1.** Operation schemes of the code, sorted by increasing computational complexity.

Operating scheme	Inversion of the lens equation	Source position	Other source parameters	Notes
Source plane	none	marginalized	marginalized	Cannot discover new images
Fast image plane	required	marginalized	marginalized	Laplace’s approximation
Standard image plane	required	free	marginalized	Exact marginalization
Full image plane	required	free	free	Rarely needed

**Notes.** `Gravity.jl` allows the user to choose the operating scheme, and to take advantage of results obtained by a simpler scheme to speed up the inference process in a more complex one through the use of the reference distribution (see Sect. 2.2.1).

Therefore, all equations found in the previous section apply, with the due variable changes, for time delay measurements. In particular, with a flat prior for  $T$  we find

$$\tau = \sum_{i=1}^I \tau_i, \quad (74)$$

$$\bar{T} = \tau^{-1} \sum_{i=1}^I \tau_i (\hat{t}_i - T_i), \quad (75)$$

and evidence

$$2 \log E_0 = \sum_{i=1}^I \left[ \log \frac{\tau_i}{2\pi} - \tau_i (\hat{t}_i - T_i - \bar{T})^2 \right] - \log \frac{\tau}{2\pi}. \quad (76)$$

## 6. Image-plane likelihood optimizations

### 6.1. Marginalized source parameters

The source-plane analysis is a powerful tool for analyzing lensing systems, as it allows us to study a lensing system relatively quickly for two main reasons: (1) we do not need to invert the lens mapping to compute the predicted images and (2) we do not need to infer over the source parameters, as these are already marginalized over. This is particularly useful when the source parameters are not of interest, which is often the case.

However, the source-plane analysis has also a possible drawback: it is essentially based on a local linearization of the lens mapping, and therefore it might not be sufficiently accurate in some situations. Additionally, it would not highlight possible issues of the lensing model, as the predictions of bright counter-images that are not observed in the data.

In these cases, it might be necessary to move to an image-plane analysis. In doing so, however, we can still take advantage of the fact that source parameters such as the source magnitude or the source reference time  $T$  appear quadratically in the log-likelihood. This allows us to perform an exact marginalization over these parameters, and to retain the source-plane likelihood only the position of each source. Specifically, the likelihood is composed of a term associated with the position, identical to Eq. (29), and to other terms associated with the other source parameters, as in Eqs. (63), (73), or (76), depending on the source type. The resulting likelihood can, as usual, be computed for the various match methods (direct association, best match, or marginalized matches). Of course, in case the source redshift is unknown, it is included as an additional free parameter.

We call this approach the standard image-plane analysis, to distinguish it from the full image-plane analysis, performed by including all source parameters in the inference. We stress that in the standard image-plane analysis there are no approximations involved.

### 6.2. Laplace’s method

A further optimization can be obtained by using Laplace’s approximation (see MacKay 2003) to avoid altogether the use of source parameters. This approach is based on a local quadratic approximation of the log-posterior around its maximum, and is therefore equivalent to assuming a normal distribution for the log-posterior. In this case, one can analytically compute the marginalization of the log-posterior over all source parameters, including the source position.

A full implementation of this method requires the computation of the local maximum of the posterior, together with its Hessian matrix. The latter is relatively easy to compute, as one can resort to automatic differentiation to compute the derivatives of the log-posterior. The former, instead, is more difficult, as it requires the solution of a nonlinear equation, with all the related issues (non-locality of the solution, convergence, etc.).

In practice, we have found that a good compromise is obtained by applying Laplace’s method with the following prescriptions:

- The maximum is computed as in Eq. (49) by taking a weighted average of the observed image positions (together with their uncertainties) mapped into the source plane;
- The inverse of the Hessian matrix is computed as Eq. (48) by mapping the precision matrix of the observed image positions into the source plane.

We note that, in this approach, that we name the “fast image-plane analysis,” we still invert the lens mapping to compute the various predicted images associated with a given source, and to compute from their positions the image-plane likelihood. However, we gain in terms of computational speed, as we do not need to include the source position as additional free parameters in the optimization process. A summary of the possible operating schemes of the code is reported synthetically in Table 1.

## 7. Technical aspects

During the implementation of `Gravity.jl`, particular care has been devoted to the numerical stability and efficiency of the code. As a result, the code is able to handle hundreds of images and lensing parameters, and to efficiently explore the parameter space. To test the performance of the code, we reconsidered a lensing system that has been studied in the literature, the “Pandora” cluster Abell 2744 (Bergamini et al. 2023a). For this system we used exactly the same data and exactly the same lens model as in the original paper, so that we could both validate the code and compare its performance with the one of `LensTool` (Kneib et al. 1996; Jullo et al. 2007), a widely used lensing code also based on the Bayesian approach. The model includes 181 halos (with 9 of them individually parametrized), 149 images divided into 50 families at more than 20 different redshifts, and 8

sources with unknown redshifts (so that their redshifts are additional free parameters); in total, the model has 50 free parameters.

The source-plane analysis of this system in `Gravity.jl` takes approximately 30 minutes on a 32-core workstation, while the fast image-plane analysis takes approximately 12 hours. The same analysis in `LensTool` takes approximately 3 weeks on a similar workstation (using, however, 100-core instead of 32, P. Bergamini, private communication). We estimate therefore a gain of a factor of  $\sim 100$  in terms of computational time. This is a remarkable result, and it opens new opportunities to study lensing systems at a level of complexity and detail that was not possible before. Below we highlight some of the technical aspects that allowed us to obtain this result.

### 7.1. Code tailoring and optimization

`Gravity.jl` is implemented in the Julia language (Bezanson et al. 2017), and therefore it benefits from the high performance of this language and of the LLVM compiler infrastructure. In particular, it takes advantage of the just-in-time compilation of the code to produce a highly optimized version of the likelihood computation, tailored to the specific lensing system under consideration. For example, `Gravity.jl` automatically detects if there is a need to update the cosmological distances (because either the redshifts or the cosmological model includes free parameters), or, in the case of multiplane lensing, if it is necessary to project the observed positions of the background lenses to obtain their real positions in the background lensing plane.

Particular care has been devoted to some technical aspects of the Julia implementation, such as the use of type-stable code, which allows the compiler to produce machine code that is as fast as C or Fortran code (avoiding one of the penalties of dynamically typed languages). Additionally, throughout the development, we used micro-benchmarking techniques for critical parts of the code (such as the computation of the lens mapping, or the inversion of the lens mapping) to optimize the various algorithms used. The same micro-benchmarking techniques are also used for some tasks at runtime to select the most efficient algorithm among a set of equivalent ones.

### 7.2. Parallelization

The code uses the parallelization capabilities of the Julia language to distribute the computation of the likelihood over multiple cores and, depending on the sampling technique used, also over distributed systems. The code also makes use of single-instruction multiple-data (SIMD) instructions when available, to further speed up the computation even in the case of a single core; to this goal, the code uses also the SLEEF library (Shibata & Petrogalli 2020).

### 7.3. Automatic differentiation

The code uses the automatic differentiation capabilities of the Julia language to compute the derivatives of the log-posterior with respect to the lensing parameters. Currently, the code uses forward-mode automatic differentiation implemented in the `ForwardDiff.jl` package (Revels et al. 2016). This allows the use of sampling techniques based on the gradient of the log-posterior, such as Hamiltonian Monte Carlo (see below Sect. 7.4).



**Fig. 3.** Lensing system HE0435–1123. As shown by this image, the lensing galaxy is a massive elliptical galaxy, surrounded by a group of galaxies. The barred spiral galaxy below the lensing galaxy is in the background. Credits: ESA/Hubble, NASA, Suyu et al.

### 7.4. Sampling techniques

The code allows for the use of different sampling techniques:

**Metropolis-Hastings.** The vanilla Metropolis-Hastings algorithm (Metropolis et al. 1953; Hastings 1970) is the simplest sampling technique. It requires careful tuning of the proposal distribution, and it is generally not very efficient.

**Affine invariant ensemble sampler.** A very efficient algorithm based on the ensemble sampler of Goodman & Weare (2010) (and known in the Python community through the library `emcee`). This algorithm is very efficient in exploring the parameter space when the posterior distribution is unimodal, which is often the case.

**Elliptical slice sampling.** Uses the algorithm proposed in Murray et al. (2010).

**Hamiltonian Monte Carlo.** The Hamiltonian Monte Carlo (HMC) algorithm is a more sophisticated sampling technique (Neal 2011; see also Betancourt 2017). It is based on the introduction of a fictitious momentum variable, which allows for a more efficient exploration of the parameter space. The use of this algorithm requires the derivative of the log-posterior, which in our code is computed using automatic differentiation. The library used in `Gravity.jl`, Xu et al. (2020), also implements the No-U-Turn Sampler (NUTS) approach of Hoffman & Gelman (2011).

**Metropolis-adjusted Langevin algorithm.** This method, called informally MALA, can be seen as an HMC algorithm with a single leap-frog time step (Rosicky et al. 1978).

**Parallel tempering.** The parallel tempering algorithm is a generalization of the Metropolis-Hastings algorithm (Swendsen & Wang 1986; Marinari & Parisi 1992). In this algorithm, several chains are run in parallel, each at a different “temperature”  $\beta$ , that is, with a modified likelihood function  $P(\mathbf{D} | \mathbf{M}, \beta) = P(\mathbf{D} | \mathbf{M})^\beta$ . When  $\beta = 0$ , the likelihood is flat, and the chain explores the prior distribution, while when

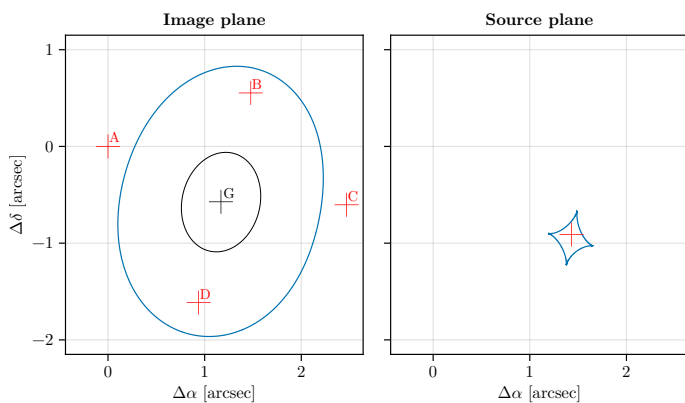


**Fig. 4.** Best-fit lensing model. **Left.** Observed image positions (red crosses) and the critical curves (blue line) for the lensing system HE0435–1123 in the singular-isothermal ellipsoid model. The black ellipse indicates the axis ratio and orientation of the main lens. **Right.** The predicted source position (red cross) and the caustic lines.

$\beta = 1$  the chain explores the posterior distribution. The algorithm alternates between a local exploration phase, when the chains are run independently, and a global exploration phase, when the chains are coupled and the states are exchanged between them. This algorithm is particularly efficient in exploring the parameter space when the posterior distribution is multimodal.

Nested sampling. The nested sampling algorithm (Skilling 2004; Chopin & Robert 2008) is a different approach to Bayesian inference. It is based on the idea of transforming the integral over the parameter space into a sum of integrals over the likelihood, and then sampling from the likelihood. The algorithm is particularly efficient in computing the evidence, and it is particularly useful when the posterior distribution is multimodal. The code uses the implementation of Lucas et al. (2021).

For completeness, `Gravity.jl` also includes robust methods to obtain the maximum likelihood or the maximum-a-posteriori solution, based on globally convergent optimization algorithms (de Dios & Mezura-Montes 2022).

### 7.5. Unit testing

The code includes an extensive suite of unit tests, which are run at each commit to the code repository. The tests cover all the critical parts of the code, such as the computation of the lens mapping, the grid algorithm, the computation of the likelihood, and the sampling techniques. The tests also include a coverage analysis, which helps us to identify parts of the code that require further testing.

## 8. HE0435–1123

As a test application for a galaxy-scale lens, we consider the lensing system HE0435–1123. This is a very well-known quadruply imaged quasar at redshift  $z_s = 1.69$  (Wisotzki et al. 2000) lensed by a foreground galaxy at redshift  $z_l = 0.454$  (Morgan et al. 2005). The system has been the subject of several studies, often focusing on the time delays between the images (Eigenbrod et al. 2006; Kochanek et al. 2006; Wong et al. 2017).

The lensing galaxy is a massive elliptical galaxy, with an Einstein radius of  $\theta_E \approx 1.61$  arcsec, but the whole system is part of a group of galaxies. The lensing system is shown in Fig. 4. Wide

Field Camera 3 (WFC3) grism observations have been used to show that the main lensing galaxy lacks significant substructures and its gravitational potential can be well described by an isothermal ellipsoid (Nierenberg et al. 2017). Therefore, in our first model, the main lensing galaxy is taken to have a singular isothermal ellipsoid mass profile (SIE). The model also includes a second lens to account for the closest perturber (a spiral galaxy in the background of the main lens, at  $z = 0.7821$ ), and a shear to account for the external field.

Since the perturber galaxy is in the background of the main lens, we need to use the full multiplane lensing equations to describe the system. We note also that in doing so, we take into account the fact that the observed position of the perturbing galaxy differs from the real position because of the gravitational lensing effect of the main galaxy.

Our lensing model includes therefore 6 parameters associated with the lensing system (which we list together with their flat prior distributions): the main lens velocity dispersion (100 .. 500 km/s), the lens axis ratio (0.25 .. 1) and position angle ( $-90^\circ$  ..  $90^\circ$ ), the external shear ( $-0.3$  ..  $0.3$  in both orientations), and the perturbing galaxy velocity dispersion (50 .. 250 km/s). The source has been modeled as a luminous point-like object, with large normal prior distributions for all parameters (the position coordinates and the magnitude). The constraints include the positions and magnitudes for the four observed point-like images; the associated data and uncertainties are taken from Morgan et al. (2005). For the magnitudes, we have used larger errors (0.1 magnitudes) to include the potential presence of microlensing effects and unaccounted luminosity variations associated with the different time delays of the various images. The model has therefore 9 free parameters (6 for the lens and 3 for the source) and 12 observational constraints.

For this system, as well as for other ones considered during the development of `Gravity.jl`, we have compared many relevant lensing properties (such as the deflection angle, the magnification, or the lensing potential) obtained with our code and with alternative programs. We have made sure that if one performs the appropriate transformations, the results obtained with different programs (including `LensTool`, Kneib et al. 1996, and `GlaGic`, Oguri 2010) are consistent, to the level of numerical precision, to each other.

Figure 5 shows the combined probability distributions for all lens parameters, obtained from a Bayesian inference in the imageplane. The log-evidence of the model has been estimated to be  $\ln Z \approx -24.2$ . These results have been obtained in less than one hour on a laptop.

For comparison, we have also considered an alternative model, where the main lens is modeled as a singular power-law ellipsoid (implemented in `Gravity.jl` through the fast algorithm of Tessore & Metcalf 2015). The posterior distribution for the various parameters is shown in Fig. 6. The first two parameters shown,  $r_e$  and  $\alpha$ , represent a generalization of the lens Einstein radius for elliptical lenses (computed from a circularized version of the mass profile) and the slope of the power-law profile,  $\kappa(x) \propto x^{\alpha-2}$ .

We note how the slope of the power-law profile is poorly constrained from these data alone, and is anyway essentially consistent with an isothermal one  $\alpha = 1$ . We note also how some parameters present rather nasty degeneracies: in particular, the Einstein radius of the main lens is strongly correlated to the slope  $\alpha$ . Curved degeneracies such as this one are particularly complicated to sample (and are in fact often used to test the performance of optimization algorithms, see, e.g., Rosenbrock 1960), but the code can handle them efficiently.

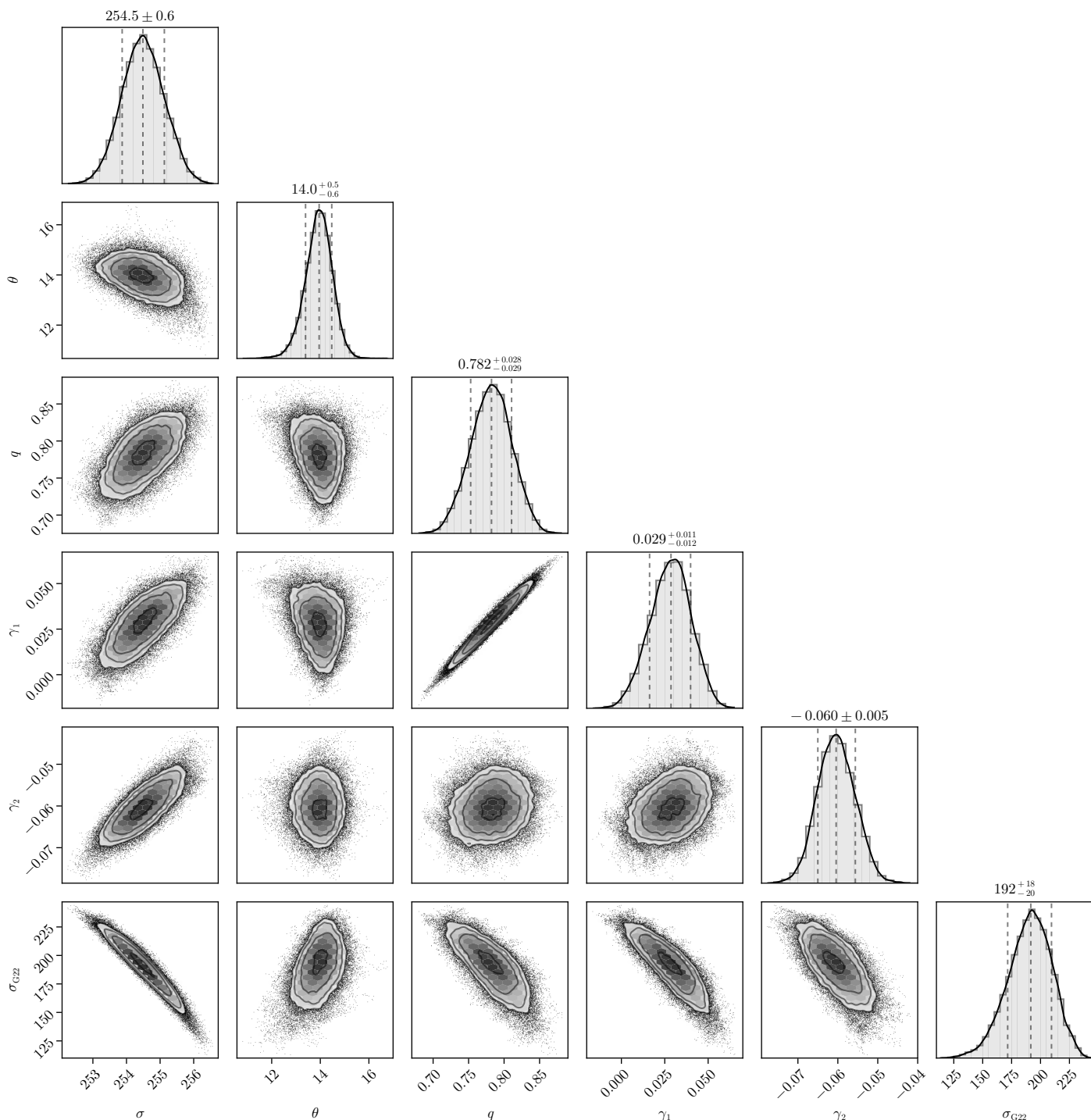


**Fig. 5.** Jointed distribution of the lensing parameters for the system HE0435–1123 in a model using a singular isothermal ellipsoid as the main lens. The contours enclose 68% and 95% of the probability.

The log-evidence associated with this model is  $\ln Z \approx -24.7$ . These results give very weak evidence in favor of the isothermal profile.

## 9. Conclusions

We have presented `Gravity.jl`, a new Julia-based code for the analysis of strong gravitational lensing systems. The code is based on a Bayesian approach, and it allows for the inference of the lensing parameters of a system, together with the marginalization of the source parameters. The code is highly parallel and

able to handle hundreds of images and lensing parameters and still efficiently explore the parameter space.

The algorithms implemented in `Gravity.jl` are all based on sound statistical frameworks, obtained through the use of the marginalization over nuisance parameters, in contrast to the use of optimizations. This allows for a robust and efficient exploration of the parameter space, and for a reliable estimation of the uncertainties associated with the lensing parameters.

In the future papers of this series, we will focus on the analysis of extended sources, for which we will consider both parametric and non-parametric models. We will also consider a com-

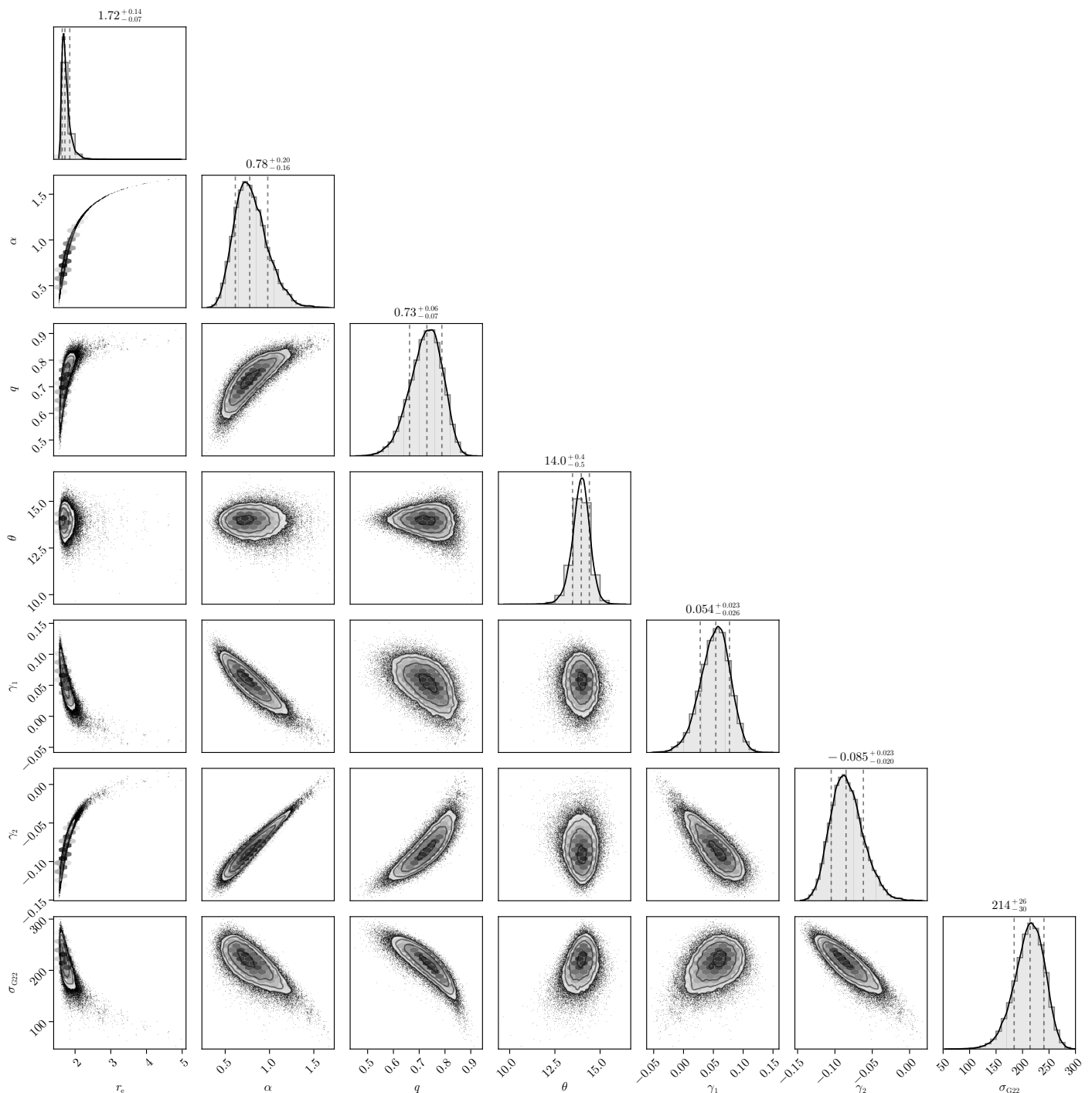


**Fig. 6.** Same as Fig. 5, but using a singular power-law mass profile for the main lens. The contours enclose 68% and 95% of the probability.

bined weak + strong lensing analysis, carried out in a way that is consistent with the Bayesian approach of the code.

*Acknowledgements.* This work has benefited from many tests, discussions, and interactions with several collaborators, including Davide Abriola, Pietro Bergamini, Claudio Grillo, Massimo Meneghetti, and Piero Rosati. We are grateful to them for their help and support.

## References

- Aycock, J. 2003, *ACM Comput. Surv.*, 35, 97–113
- Bergamini, P., Acebron, A., Grillo, C., et al. 2023a, *ApJ*, 952, 84
- Bergamini, P., Grillo, C., Rosati, P., et al. 2023b, *A&A*, 674, A79
- Betancourt, M. 2017, arXiv e-prints, arXiv:1701.02434
- Bezanson, J., Edelman, A., Karpinski, S., & Shah, V. B. 2017, *SIAM review*, 59, 65
- Blanchard, P., Higham, D. J., & Higham, N. J. 2020, *IMA Journal of Numerical Analysis*, 41, 2311
- Caminha, G. B., Grillo, C., Rosati, P., et al. 2016, *A&A*, 587, A80
- Caminha, G. B., Suyu, S. H., Grillo, C., & Rosati, P. 2022, *A&A*, 657, A83
- Chopin, N. & Robert, C. 2008, arXiv e-prints, arXiv:0801.3887
- de Dios, J.-A. M. & Mezura-Montes, E. 2022, *Journal of Open Source Software*, 7, 4723
- Eigenbrod, A., Courbin, F., Meylan, G., Vuissoz, C., & Magain, P. 2006, *A&A*, 451, 759
- Goodman, J. & Weare, J. 2010, *Communications in Applied Mathematics and Computational Science*, 5, 65
- Grillo, C., Pagano, L., Rosati, P., & Suyu, S. H. 2024, *A&A*, 684, L23
- Grillo, C., Suyu, S. H., Rosati, P., et al. 2015, *ApJ*, 800, 38
- Hastings, W. K. 1970, *Biometrika*, 57, 97

- Hilbert, S., Hartlap, J., White, S. D. M., & Schneider, P. 2009, *A&A*, 499, 31
- Hoffman, M. D. & Gelman, A. 2011, arXiv e-prints, arXiv:1111.4246
- Johnson, T. L. & Sharon, K. 2016, *ApJ*, 832, 82
- Jullo, E., Kneib, J. P., Limousin, M., et al. 2007, *New Journal of Physics*, 9, 447
- Kneib, J. P., Ellis, R. S., Smail, I., Couch, W. J., & Sharples, R. M. 1996, *ApJ*, 471, 643
- Kochanek, C. S., Morgan, N. D., Falco, E. E., et al. 2006, *ApJ*, 640, 47
- Lattner, C. & Adve, V. 2004, in *Proceedings of the International Symposium on Code Generation and Optimization: Feedback-Directed and Runtime Optimization, CGO '04 (USA: IEEE Computer Society)*, 75
- Livan, G., Novaes, M., & Vivo, P. 2018, *Introduction to random matrices*, 1st edn., *SpringerBriefs in Mathematical Physics* (Cham, Switzerland: Springer International Publishing)
- Lucas, M., Kaur, S., Fjelde, T. E., et al. 2021, *TuringLang/NestedSamplers.jl: v0.8.1*
- MacKay, D. 2003, *Information Theory, Inference, and Learning Algorithms* (Cambridge University Press)
- Mahalanobis, P. C. 1936, *Journ. Asiatic Soc. Bengal*, XXVI, 541
- Marinari, E. & Parisi, G. 1992, *EPL (Europhysics Letters)*, 19, 451
- Metropolis, N., Rosenbluth, A. W., Rosenbluth, M. N., Teller, A. H., & Teller, E. 1953, *Journal of Chemical Physics*, 21, 1087
- Morgan, N. D., Kochanek, C. S., Pevunova, O., & Schechter, P. L. 2005, *AJ*, 129, 2531
- Murray, I., Adams, R., & MacKay, D. 2010, in *Proceedings of Machine Learning Research, Vol. 9, Proceedings of the Thirteenth International Conference on Artificial Intelligence and Statistics*, ed. Y. W. Teh & M. Titterton (Chia Laguna Resort, Sardinia, Italy: PMLR), 541–548
- Neal, R. 2011, in *Handbook of Markov Chain Monte Carlo*, 113–162
- Nierenberg, A. M., Treu, T., Brammer, G., et al. 2017, *MNRAS*, 471, 2224
- Oguri, M. 2010, *PASJ*, 62, 1017
- Oguri, M. 2021, *PASP*, 133, 074504
- Priewe, J., Williams, L. L. R., Liesenborgs, J., Coe, D., & Rodney, S. A. 2017, *MNRAS*, 465, 1030
- Revels, J., Lubin, M., & Papamarkou, T. 2016, arXiv:1607.07892 [cs.MS]
- Rosenbrock, H. H. 1960, *The Computer Journal*, 3, 175
- Rosky, P. J., Doll, J. D., & Friedman, H. L. 1978, *The Journal of Chemical Physics*, 69, 4628
- Seitz, S. & Schneider, P. 1992, *A&A*, 265, 1
- Shibata, N. & Petrogalli, F. 2020, *IEEE Transactions on Parallel and Distributed Systems*, 31, 1316
- Skilling, J. 2004, in *American Institute of Physics Conference Series, Vol. 735, Bayesian Inference and Maximum Entropy Methods in Science and Engineering: 24th International Workshop on Bayesian Inference and Maximum Entropy Methods in Science and Engineering*, ed. R. Fischer, R. Preuss, & U. V. Toussaint (AIP), 395–405
- Swendsen, R. H. & Wang, J.-S. 1986, *Phys. Rev. Lett.*, 57, 2607
- Tessore, N. & Metcalf, R. B. 2015, *A&A*, 580, A79
- Treu, T. 2010, *ARA&A*, 48, 87
- Treu, T., Suyu, S. H., & Marshall, P. J. 2022, *A&A Rev.*, 30, 8
- Wishart, J. 1928, *Biometrika*, 20A, 32
- Wisotzki, L., Christlieb, N., Bade, N., et al. 2000, *A&A*, 358, 77
- Wong, K. C., Suyu, S. H., Auger, M. W., et al. 2017, *MNRAS*, 465, 4895
- Xu, K., Ge, H., Tebbutt, W., et al. 2020, in *Symposium on Advances in Approximate Bayesian Inference*, PMLR, 1–10



**Appendix A: YAML configuration file**

```

cosmology:
  Omega_m: 0.3
  h_0: 0.7
  Omega_r: 0.0
  w_0: -1
sampling:
  scheme: sourceplane
  likelihood-options:
    bayesianfactor: true
    matches: all
    duplicates: true
    missedpredictionpenalty: true
    fitsource: true
  algorithm: hmc
  algorithm-options:
    method: NUTS
    warmup: 5000
    iterations: 50000
  threads: auto
  random-seed: 1
lenses:
  - NIE:
    name: main
    z: z_lens
    x: x_lens
    sigma: 100 .. 500
    s: 0.0
    theta: -pi/2 .. pi/2
    q: 0.25 .. 1
  - Shear:
    name: shear
    z: z_lens
    x: x_lens
    gamma: (-0.3, -0.3) .. (0.3, 0.3)
  - SIS:
    name: G22
    z: z_G22
    x: x_G22
    sigma: 50 .. 250
sources:
  - Luminous:
    z: 1.689
    x: (0.0, 0.0) ± 10.0
    mag: 20.0 ± 10.0
    images:
      - Luminous:
        x: (0.0, 0.0) ± 0.002
        mag: 18.545 ± 0.1
      - Luminous:
        x: (-2.4687, -0.6033) ± 0.002
        mag: 19.082 ± 0.1
      - Luminous:
        x: (-1.4772, 0.5532) ± 0.002
        mag: 19.149 ± 0.1
      - Luminous:
        x: (-0.9377, -1.6147) ± 0.002
        mag: 19.196 ± 0.1

```